Chinese Chemical Letters 35 (2024) 108663

Contents lists available at ScienceDirect

Chinese Chemical Letters

journal homepage: www.elsevier.com/locate/cclet

Heavy-atom engineered hypoxia-responsive probes for precisive photoacoustic imaging and cancer therapy

Ling-Ling Wu[a,b,1], Xiangchuan Meng[b,1], Qingyang Zhang[b], Xiaowan Han[b], Feiya Yang[a], Qinghua Wang[b,*], Hai-Yu Hu[b,*], Nianzeng Xing[a,*]

[a] Department of Urology, National Cancer Center/National Clinical Research Center for Cancer/Cancer Hospital, Chinese Academy of Medical Sciences and Peking Union Medical College, Beijing 100021, China
[b] State Key Laboratory of Bioactive Substances and Function of Natural Medicine, Institute of Materia Medica, Peking Union Medical College and Chinese Academy of Medical Sciences, Beijing 100050, China

ARTICLE INFO

Article history:
Received 10 May 2023
Revised 5 June 2023
Accepted 7 June 2023
Available online 11 June 2023

Keywords:
Heavy-atom effect
Phototherapy
Photoacoustic imaging
Hypoxia-responsive
Prostate cancer

ABSTRACT

Photoacoustic agents combining photodynamic therapy (PDT) and photothermal therapy (PTT) functions have emerged as potent theranostic agents for combating cancer. The molecular approaches for enhancing the near-infrared (NIR)-absorption and maximizing non-radiative energy transfer are essential for effective photoacoustic imaging (PAI) and therapy applications. In addition, such molecules with high specificity and affinity to cancer cells are urgently needed, which would further decrease the side effect during treatments. In this study, we applied a heavy-atom engineering strategy and introduced *p*-aminophenol, -thio, and -seleno moieties into NIR heptamethine cyanine (Cy7) skeleton (Cy7-X-NH_2, X = O, S, Se) to significantly increase photothermal conversion efficiency for PTT and promote intersystem crossing for PDT. Additionally, we designed a series of nitroreductase (NTR)-activated photoacoustic probes (Cy7-X-NO_2, X = O, S, Se), and target hypoxic tumors with NTR overexpression. Our prostate cancer targeting probe, Cy7-Se-NO_2-KUE, exhibited specific tumor photoacoustic signals and effective tumor killing through outstanding synergistic PTT/PDT *in vivo*. These findings highlighted a versatile strategy for cancer photoacoustic diagnosis and enhanced phototherapy.

Cancer is a significant global health issue, with 19.3 million new cases and 10 million cancer-related deaths reported worldwide in 2020 [1]. To develop more effective and accurate treatments for cancer, researchers worldwide have been dedicated to addressing this challenge. Traditional cancer therapies, such as surgery, radiotherapy, and chemotherapy, are associated with drawbacks like immune system damage, drug resistance, and the killing of normal cells [2–5]. Therefore, alternative and tolerable tumor therapy strategies are urgently needed. Phototherapy, including photodynamic therapy (PDT) and photothermal therapy (PTT), is a promising tumor therapy method that converts light energy into localized hyperthermia inducing heat shock, and generates cytotoxic reactive oxygen species (ROS) for ablating tumor cells [6–12]. However, as a non-invasive therapeutic strategy, phototherapy is restricted by light irradiation with minimal toxicity on normal tissues, damaging a wide range of cells including multidrug cancer, and stimulating an immune response by inducing cell apoptosis or necrosis [13]. Photosensitizers (PSs) are a crucial component of phototherapy. Inorganic materials, while possessing excellent photothermal conversion efficiencies and photo-stabilities, have limited clinical translation due to their poor biodegradability and long-term toxicity [14,15]. Therefore, organic PSs with biocompatibility and low cytotoxicity have been developed through dedicated synthesis to enhance the outcome of phototherapy [6,16–19].

Cyanine derivatives, with excellent biosafety, high molar extinction coefficient, and deep tissue penetration depth, have been considered superior potential candidates for modification into phototherapy agents [20–23]. Based on mitochondria sensitive to heat shock and the inherent anchoring of cyanine analogues with positive charge in mitochondria [24–27], we designed a mitochondria nitroreductase (NTR)-activated photoacoustic probe that utilized the photoinduced electron transfer (PeT) mechanism to enhance photothermal conversion efficiency for PTT, and incorporated heavy atoms into the cyanine chromophore could efficiently facilitate intersystem crossing (ISC) and ROS generation for PDT

* Corresponding authors.
E-mail addresses: wangqinghua@imm.ac.cn (Q. Wang), haiyu.hu@imm.ac.cn (H.-Y. Hu), xingnianzeng@126.com (N. Xing).
[1] These authors contributed equally to this work.

https://doi.org/10.1016/j.cclet.2023.108663
1001-8417/

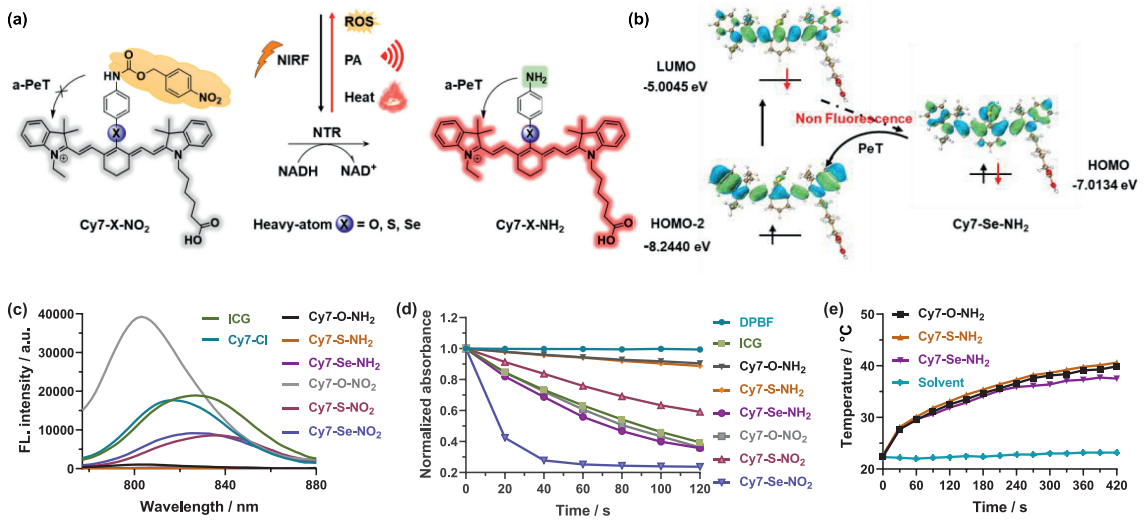

Fig. 1. (a) Structures of Cy7-X-NH_2 and Cy7-X-NO_2 (X = O, S, Se), and response mechanism of Cy7-X-NO_2 toward NTR. (b) Calculated HOMO/LUMO distribution of Cy7-Se-NH_2 based on DFT method. (c) Fluorescence emission spectra of ICG, Cy7-Cl, Cy7-X-NH_2, and Cy7-X-NO_2 (X = O, S, Se) (10 μmol/L) in DMSO, λ_{ex} = 740 nm. (d) Normalized absorbance changes of DPBF at 415 nm in the presence of ICG, Cy7-X-NH_2, and Cy7-X-NO_2 (X = O, S, Se) under a 785 nm irradiation (200 mW/cm^2, 2 min). (e) Temperature changes of Cy7-X-NH_2 (X = O, S, Se) (20 μmol/L) in DMSO irradiated with 785 nm light (800 mW/cm^2, 7 min).

used for efficiently killing tumor cells synergistically. Consequently, we synthesized Cy7-O-NO_2, Cy7-S-NO_2, and Cy7-Se-NO_2 as NTR-activated photoacoustic probes for PTT. Notably, Cy7-Se-NO_2 exhibited superior ROS generation capability compared to indocyanine green (ICG) as a PDT agent. We introduced prostate-specific membrane antigen (PSMA)-specific targeting groups KUE (Lys-urea-Glu) into Cy7-Se-NO_2, structured Cy7-Se-NO_2-KUE for aiming to improve NTR enzyme activation, achieve prostate cancer (PCa) specific imaging, and efficiently kill tumors *in vivo* through synergistic PTT/PDT. This strategy provided an efficient tool for the specific diagnosis and phototherapy of tumors.

Introducing heavy atoms is a widely used approach to enhance the ISC and the generation of ROS [13,28–30]. Moreover, the incorporation of aminophenol to the *meso*–position of cyanine dyes conjugated polymethine backbone could contribute to quench fluorescence [31]. As well, sulfur and selenium substitution could further extend the absorption wavelengths [32,33]. These findings led to the development of a series of near-infrared (NIR) PSs (Cy7-O-NH_2, Cy7-S-NH_2, and Cy7-Se-NH_2) with *p*-aminophenol, -thio, and -seleno substitution at the *meso*–position based on heptamethine cyanines (Cy7). These were then amidated with a specific NTR cleavable group (*p*-nitrobenzyl chloroformate) to construct activable probes (Cy7-O-NO_2, Cy7-S-NO_2, and Cy7-Se-NO_2) (Fig. 1a). These probes were designed with several advantages: (1) Introduction of *p*-aminophenol, -thio, and -seleno promoted non-radiative relaxation pathways to generate further wavelengths red-shift, low fluorescence quantum yield, and obvious photothermal effect; (2) Selenium atom enhanced spin-orbit coupling, which facilitated the ISC from a singlet state to a triplet state, resulting in highly cytotoxic $^1O_2$ to kill cancer cells by PDT; (3) The heat sensitivity of tumor mitochondria and the inherent targeting of probes to mitochondria were conducive to enrichment in tumors and to achieve a highly effective and specific antitumor effect by PTT. To further improve the targeting for PCa, the probe Cy7-Se-NO_2-KUE was linked with a PSMA-specific ligand KUE (PSMA was highly expressed in both primary PCa and lymph node metastasis compared with normal tissues). The overexpression of NTR in solid tumors reduced the *p*-nitrobenzyl chloroformate group [34], releasing Cy7-Se-NH_2-KUE through a rearrangement and elimination mechanism, generating enhanced photoacoustic (PA) signal output to visualize the tumor region *in vivo* and achieving a significant antitumor effect through combined PTT and PDT.

As a preliminary step, we synthesized Cy7-O-NH_2, Cy7-S-NH_2, Cy7-Se-NH_2, Cy7-O-NO_2, Cy7-S-NO_2, and Cy7-Se-NO_2, using the synthetic routes outlined in Scheme S1 (Supporting information). These chemical structures were confirmed by ^1H nuclear magnetic resonance (NMR), ^{13}C NMR, and high-resolution mass spectra (HRMS). To assess the potential of these compounds (Cy7-O-NH_2, Cy7-S-NH_2, and Cy7-Se-NH_2) act as NIR PSs, firstly, we analyzed their absorption and emission spectra in DMSO, along with those of ICG and Cy7-Cl, as shown in Fig. 1c and Fig. S1 (Supporting information). All the compounds displayed broad NIR absorption bands (>300 nm) with strong absorption (large molar extinction coefficients, $\varepsilon = 16.8 \times 10^4 - 21.2 \times 10^4$ L mol^{-1} cm^{-1}) and maximum absorption wavelength over 780 nm, indicating excellent light trapping capability and deeper penetration depth in tissues for therapeutic action. Upon introducing heavy atoms, such as sulfur and selenium, the maximum absorption wavelengths of Cy7-S-NH_2 and Cy7-Se-NH_2 were increased by 12 and 4 nm, respectively, compared to Cy7-Cl (λ_{abs} = 794 nm) (Fig. S2 in Supporting information), while their corresponding fluorescence emissions were red-shifted from 815 nm to 837 and 827 nm. For Cy7-O-NH_2, both maximum absorption and emission wavelengths were weak blue-shifted to 782 and 803 nm, respectively. As expected, Cy7-O-NH_2, Cy7-S-NH_2, and Cy7-Se-NH_2 exhibited extremely weak fluorescence emissions, with fluorescence quantum yields (Φ_f) as low as 0.86%, 0.32%, and 0.29%, respectively, attenuating 93.0%, 97.4%, and 97.7% compared to ICG (Φ_f = 12.35% in DMSO) (Table S1 in Supporting information), indicating the radiative relaxation pathways were weak in these compounds, and non-radiative relaxation pathways were dominant, making them efficient in PTT and/or PDT.

Then, the NTR-activated probes Cy7-O-NO_2, Cy7-S-NO_2, and Cy7-Se-NO_2 were investigated, their maximum absorption and fluorescence emission wavelengths were found to be similar to those of the reduced products (Fig. 1c and Fig. S1), and their fluorescence intensities were restored by a factor of 37, 45, and 36, respectively. The fluorescence quantum yields of these probes were measured to be 20.76%, 8.18%, and 9.06%, respectively (Table S1), demonstrated the blockage of the photo-induced electron transfer (PeT) effect produced by the introduction of *p*-aminophenol, -thio,

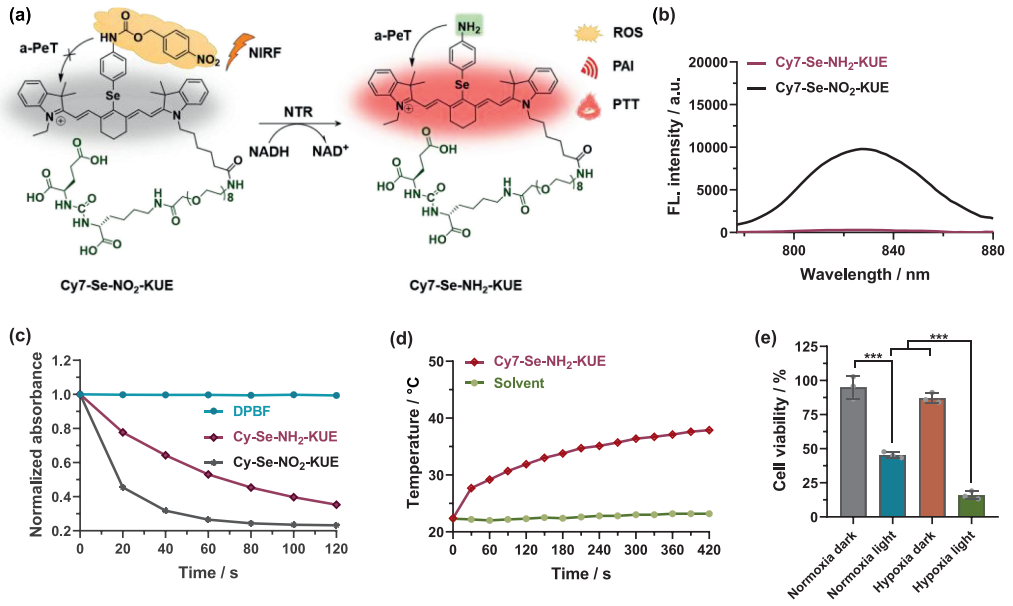

Fig. 2. (a) Structures of Cy7-Se-NO_2-KUE and Cy7-Se-NH_2-KUE, and response mechanism of Cy7-Se-NO_2-KUE toward NTR. (b) Fluorescence emission spectra of Cy7-Se-NO_2-KUE and Cy7-Se-NH_2-KUE (10 μmol/L) in DMSO, $\lambda_{ex} = 740$ nm. (c) Normalized absorbance changes of DPBF at 415 nm in the presence of Cy7-Se-NO_2-KUE and Cy7-Se-NH_2-KUE under a 785 nm irradiation (200 mW/cm^2, 2 min). (d) Temperature changes of Cy7-Se-NH_2-KUE (20 μmol/L) in DMSO irradiated with 785 nm light (800 mW/cm^2, 7 min). (e) Cytotoxicity evaluation of Cy7-Se-NO_2-KUE at 20 μmol/L against C4–2 cells with or without 808 nm laser irradiation in both normoxia and hypoxia conditions. mean ± standard deviation (S.D., $n = 3$), $^{***}P < 0.001$.

and -seleno groups. To better explain the fluorescence quenching phenomenon, we theoretically calculated spatial distributions of the highest occupied molecular orbital (HOMO) and lowest unoccupied molecular orbital (LUMO) levels of Cy7-O-NH_2, Cy7-S-NH_2, and Cy7-Se-NH_2 (Fig. 1b and Fig. S3 in Supporting information). Our results showed that, under photoexcitation, electron transited from HOMO-2 to LUMO of Cy7 core, the HOMO level of *p*-aminophenol, -thio, and -seleno moiety was higher than HOMO-2 of Cy7 core slightly, which contributed to a one-electron transfer from *p*-aminophenol, -thio, and -seleno moiety to Cy7 core, and the energy decayed through an internal conversion process that suppressed the radiative relaxation leading to fluorescence quenching.

Excellent ROS generation ability is necessary for PSs, the $^1O_2$ generation ability was tested under 785 nm light (200 mW/cm^2) using 1,3-diphenylisobenzofuran (DPBF) as a $^1O_2$ indicator. As shown in Fig. 1d, the DPBF absorption intensity changes were recorded every 20 s, the DPBF intensities were down to 39%, 90%, 89%, 36%, 36%, 59%, and 24%, respectively within 2 min in the presence of ICG, Cy7-O-NH_2, Cy7-S-NH_2, Cy7-Se-NH_2, Cy7-O-NO_2, Cy7-S-NO_2, or Cy7-Se-NO_2. Notably, Cy7-Se-NO_2 exhibited the highest $^1O_2$ quantum yield ($\Phi_\Delta = 29.8\%$), which was 4 times that of ICG ($\Phi_\Delta = 7.7\%$ [35]), and the $^1O_2$ quantum yield of Cy7-Se-NH_2 ($\Phi_\Delta = 8.5\%$) was also comparable to that of ICG (Table S1). This indicated that the selenium atom of Cy7-Se-NO_2 and Cy7-Se-NH_2 facilitated the generation of highly cytotoxic $^1O_2$. Furthermore, we measured the ROS generation efficiency in Tris-HCl buffer using ROS capture compound, 2′,7′-dichlorodihydrofluorescein diacetate (DCFH-DA) with the same light conditions (Fig. S4 in Supporting information), and found that all the probes showed enhanced ROS generation ability than ICG. We also investigated the photothermal effects of Cy7-O-NH_2, Cy7-S-NH_2, and Cy7-Se-NH_2 by detecting the temperature changes in DMSO irradiated with 785 nm light (800 mW/cm^2, 7 min) (Fig. 1e). The results showed that these compounds possessed significant photothermal effects and high-efficiency of photothermal conversion, with temperature rising by 6.7 °C, 17.4 °C, and 14.3 °C, respectively. We then measured the reactivity of Cy7-O-NO_2, Cy7-S-NO_2, and Cy7-Se-NO_2 toward NTR in Tris-HCl buffer solution (Fig. S5 in Supporting information), and found that their fluorescence intensities were partially decreased in aqueous solution due to their poor water-solubility, which affected the catalytic activity of NTR.

In light of the excellent $^1O_2$ generation ability and significant photothermal effect of Cy7-Se-NO_2, further investigation was warranted. To enhance the water solubility and increase specific uptake in PCa tissues, Cy7-Se-NO_2 was assembled with a PSMA ligand KUE *via* a polyethylene glycol (PEG)-chain linker to prepare probe Cy7-Se-NO_2-KUE (Fig. 2a), and the reduced product Cy7-Se-NH_2-KUE was also constructed. The absorption and emission spectra, molar extinction coefficients, fluorescence quantum yields, and $^1O_2$ quantum yields of Cy7-Se-NO_2-KUE and Cy7-Se-NH_2-KUE were measured in DMSO (Figs. 2b and c, Fig. S6 in Supporting information), the results showed no significant differences from the precursors (Cy7-Se-NO_2 and Cy7-Se-NH_2). Furthermore, Cy7-Se-NH_2-KUE displayed a significant temperature increase from 22.4 °C to 37.9 °C when exposed to 785 nm irradiation, whereas the temperature of the solvent without the probe only increased by 0.9 °C (Fig. 2d).

In order to verify the response of Cy7-Se-NO_2-KUE to NTR, the fluorescence emission spectra were studied and analyzed. Cy7-Se-NO_2-KUE was incubated with NTR in the presence of NADH (beta-nicotinamide adenine dinucleotide disodium salt hydrate, reduced form), and the fluorescence intensity at 810 nm gradually decreased over incubation time leading to the formation of Cy7-Se-NH_2-KUE. Cy7-Se-NO_2-KUE exhibited better enzymatic activity than Cy7-Se-NO_2 due to water solubility improvement (Fig. S7 in Supporting information). In preparation for *in vivo* experiments, we evaluated the cytotoxicity of Cy7-Se-NO_2-KUE and Cy7-Se-NH_2-KUE using a standard cell counting kit-8 (CCK-8) assay in two types of PCa cells: C4–2 cells (PSMA high-expressed) and PC3 cells (PSMA negative-expressed). The result manifested that both Cy7-Se-NO_2-KUE and Cy7-Se-NH_2-KUE exhibited no cytotoxicity up to 25 μmol/L concentrations (Fig. S8 in Supporting information). We then assessed the photocytotoxicity and dark cytotoxicity of Cy7-Se-NO_2-KUE under normoxia (21% O_2) and hypoxia (1% O_2) conditions against C4–2 cells (Fig. S9 in Supporting infor-

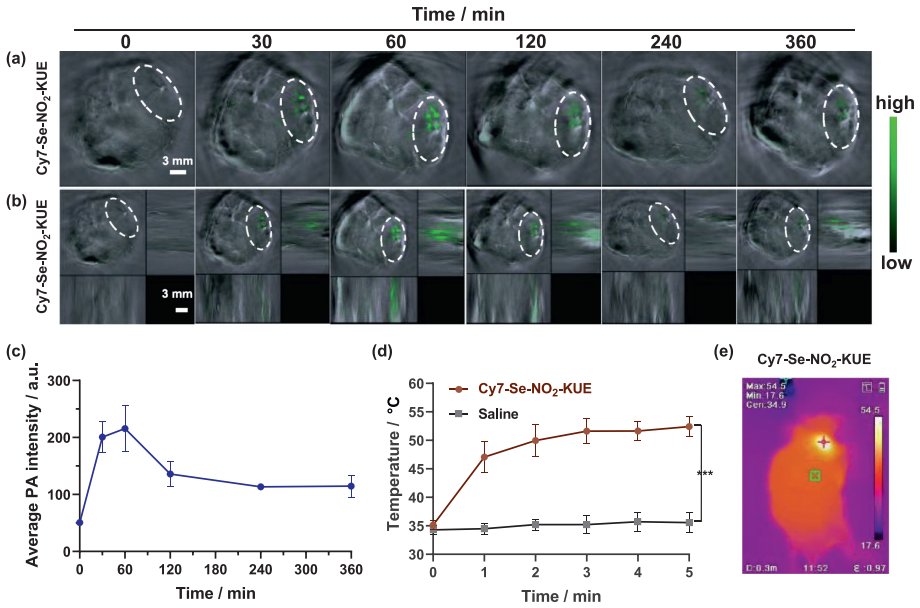

Fig. 3. *In vivo* tumor PA imaging and photothermal response. (a) PA images of C4–2 tumor-bearing nude mice at 0, 30, 60, 120, 240, and 360 min after intratumoral injection of Cy7-Se-NO_2-KUE (20 μmol/L, 50 μL). Scale bar: 3 mm. (b) Corresponding 3D reconstruction images of tumor region after 0, 30, 60, 120, 240, and 360 min treatment. Scale bar: 3 mm. (c) The quantitative PA intensities at 795 nm of tumor region at different time points ($n = 5$). (d) The temperature changes of tumor region under 785 nm irradiation (800 mW/cm^2) for 5 min after 1 h incubation with Cy7-Se-NO_2-KUE (20 μmol/L, 50 μL) or saline (50 μL). mean ± S.D. ($n = 5$), $^{***}P < 0.001$. (e) Infrared thermal image of tumor region under 785 nm irradiation at 3 min time point treated with Cy7-Se-NO_2-KUE. The red cross means the temperature measuring point in the tumor region.

mation). The dark cytotoxicity of Cy7-Se-NO_2-KUE was not apparent at different concentrations (0–20 μmol/L) under both normoxia and hypoxia. In contrast, the cell viability decreased significantly when treated with Cy7-Se-NO_2-KUE under 808 nm light irradiation (800 mW/cm^2, 5 min), indicating a strong antitumor effect on cancer cells. In particular, an enhanced photocytotoxicity was observed in hypoxia compared to normoxia (Fig. 2e) due to higher expression of NTR in hypoxia, allowing for the release of more PSs, Cy7-Se-NH_2-KUE. These results confirmed Cy7-Se-NO_2-KUE could induce a significant antitumor effect under irradiation and exhibit low dark cytotoxicity.

To investigate the behavior of Cy7-Se-NO_2-KUE toward tumor *in vivo*, we performed PA imaging to visualize its distribution in subcutaneous C4–2 tumors bearing-model of nude mice (all the animal procedures were approved by the Ethics Committee for Animal Experiments of Institute of Materia Medica, Chinese Academy of Medical Sciences & Peking Union Medical College, Approval No. 00007705) (Figs. 3a–c and Fig. S10 in Supporting information). Following intratumoral administration of Cy7-Se-NO_2-KUE (20 μmol/L, 50 μL) in PCa mice model, the PA signals were observed mainly in the tumor region and gradually intensified over time, peaking at 1 h after treatment. This observation indicated that Cy7-Se-NO_2-KUE was captured in tumors and could produce an enhanced PA signal output, enabling visualization of the tumor region. On account of the PA signals in the tumor region reaching maximal intensity at 1 h post-injection, we tested the *in vivo* photothermal effect in C4–2 xenograft tumors at this time point. C4–2 xenograft tumor mice were irradiated with a 785 nm laser (800 mW/cm^2) for 5 min, resulting in a gradual increase in tumor temperature over the irradiation time. and tumor temperature reached a plateau at 3 min with a final temperature of 52 °C. This temperature was sufficient to trigger cancer cell ablation and was 17 °C higher than that of the control group treated with saline (Figs. 3d and e, Fig. S11 in Supporting information). These results suggested that Cy7-Se-NO_2-KUE had potential as a photothermal agent for cancer therapy *in vivo*.

To evaluate the therapeutic efficacy of Cy7-Se-NO_2-KUE *in vivo*, we investigated its phototherapy capacity in a C4–2 xenograft tumor model. The therapeutic outcome was assessed by continuously monitoring the tumor growth rates. As described in Figs. 4a and c, and Figs. S12 and S13 (Supporting information), significant tumor inhibition and size reduction were observed when tumors treated with both Cy7-Se-NO_2-KUE (20 μmol/L, 50 μL) and laser irradiation. Conversely, negligible tumor inhibition was observed in the other three control groups, and neither Cy7-Se-NO_2-KUE alone nor irradiation alone exhibited any notable inhibition of tumor growth. No obvious changes in mice body weight were observed among all groups during the treatment (Fig. 4b). After treatment, we performed hematoxylin-eosin (H&E) staining of dissected tumor tissues in all groups, and only cells in tumors treated with both Cy7-Se-NO_2-KUE and irradiation were severely destroyed (Fig. 4d). Additionally, we found no apparent histopathological variation in hearts, livers, spleens, lungs, and kidneys, along with excellent plasma stability (Figs. S14 and S15 in Supporting information), demonstrating that the excellent biocompatibility and safety of Cy7-Se-NO_2-KUE *in vivo* systems. Therefore, our results demonstrated that Cy7-Se-NO_2-KUE had great potential as a phototherapeutic agent for treating PCa *in vivo*.

In conclusion, we investigated a range of activated-PSs including Cy7-O-NO_2, Cy7-S-NO_2, and Cy7-Se-NO_2, which demonstrated not only excellent ability in generating $^1O_2$ for PDT by itself but also significant photothermal effects for PTT after reduced by NTR. Among them, we further explored the potential of Cy7-Se-NO_2-KUE as a powerful tool for the diagnosis and treatment of PCa by synergistic PTT/PDT. *In vivo* experiments demonstrated that Cy7-Se-NO_2-KUE efficiently diagnosed and killed PCa tumors *via* the enhanced PA signal output and the synergistic effect of PTT and PDT. Importantly, our results also revealed the biocompatibility and safety of Cy7-Se-NO_2-KUE *in vivo*, highlighting its promising application in the field of cancer diagnosis and treatment.

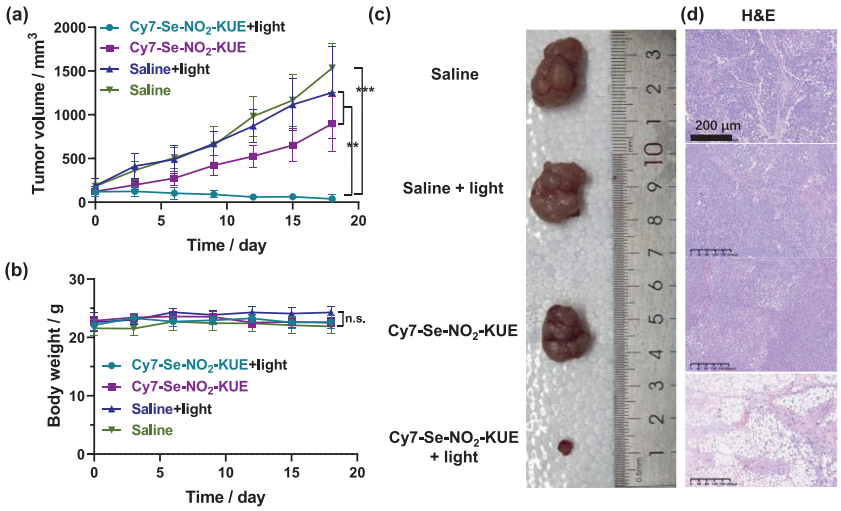

Fig. 4. *In vivo* tumor phototherapy. (a) Tumor volume and (b) body weight changes during 18-day treatment. mean ± S.D. ($n = 5$), $^{**}P < 0.01$, $^{***}P < 0.001$, n.s. represents no significant difference. (c) Images of tumor dissected from mice in different treatment groups after 18-day treatment. (d) H&E stained tumors images in different treatment groups. Scale bar: 200 μm.

Declaration of competing interest

The authors declare that they have no known competing financial interests or personal relationships that could have appeared to influence the work reported in this paper.

Acknowledgments

This work was partially supported by the National Key R&D Program of China (No. 2022YFE0199700), the National Natural Science Foundation of China (NSFC) projects (Nos. 22077139 and 22122705), and CAMS Innovation Fund for Medical Sciences (CIFMS) (No. 2022-I2M-2–002).

Supplementary materials

Supplementary material associated with this article can be found, in the online version, at doi:10.1016/j.cclet.2023.108663.

References

[1] H. Sung, J. Ferlay, R.L. Siegel, et al., CA Cancer J. Clin. 71 (2021) 209–249.
[2] X. Chen, F. Cheng, Y. Liu, et al., EBioMedicine 40 (2019) 135–150.
[3] G. Galletti, B.I. Leach, L. Lam, S.T. Tagawa, Cancer Treat Rev. 57 (2017) 16–27.
[4] A. Martini, G. Gandaglia, N. Fossati, et al., Eur. Urol. Oncol. 4 (2021) 42–48.
[5] M.C. Vozenin, J. Bourhis, M. Durante, Nat. Rev. Clin. Oncol. 19 (2022) 791–803.
[6] K. Li, S. Xu, M. Xiong, et al., Chem. Soc. Rev. 50 (2021) 11766–11784.
[7] Z. Xie, T. Fan, J. An, et al., Chem. Soc. Rev. 49 (2020) 8065–8087.
[8] C. Xu, R. Ye, H. Shen, et al., Angew. Chem. Int. Ed. 61 (2022) e202204604.
[9] J. Zhang, L. Ning, J. Huang, C. Zhang, K. Pu, Chem. Sci. 11 (2019) 618–630.
[10] H. Zhao, N. Li, C. Ma, et al., Chin. Chem. Lett. 34 (2023) 107699.
[11] Z. Cheng, T. Zhang, W. Wang, et al., Chin. Chem. Lett. 32 (2021) 1580–1585.
[12] X. Li, R. Luo, X. Liang, Q. Wu, C. Gong, Chin. Chem. Lett. 33 (2022) 2213–2230.
[13] T.C. Pham, V.N. Nguyen, Y. Choi, S. Lee, J. Yoon, Chem. Rev. 121 (2021) 13454–13619.
[14] L. Gourdon, K. Cariou, G. Gasser, Chem. Soc. Rev. 51 (2022) 1167–1195.
[15] X. Li, M. Yang, J. Cao, et al., ACS Mater. Lett. 4 (2022) 724–732.
[16] W. Chen, Z. Wang, M. Tian, et al., J. Am. Chem. Soc. 145 (2023) 8130–8140.
[17] W. Hu, P.N. Prasad, W. Huang, Acc. Chem. Res. 54 (2021) 697–706.
[18] H. Li, Y. Kim, H. Jung, J.Y. Hyun, I. Shin, Chem. Soc. Rev. 51 (2022) 8957–9008.
[19] Q. Ma, X. Sun, W. Wang, et al., Chin. Chem. Lett. 33 (2022) 1681–1692.
[20] L. Li, X. Han, M. Wang, et al., Chem. Eng. J. 417 (2021) 128844.
[21] Y. Liu, P. Bhattarai, Z. Dai, X. Chen, Chem. Soc. Rev. 48 (2019) 2053–2108.
[22] B.M. Vickerman, E.M. Zywot, T.K. Tarrant, D.S. Lawrence, Nat. Rev. Chem. 5 (2021) 816–834.
[23] X. Zhao, J. Liu, J. Fan, H. Chao, X. Peng, Chem. Soc. Rev. 50 (2021) 4185–4219.
[24] X. Guo, N. Yang, W. Ji, et al., Adv. Mater. 33 (2021) e2007778.
[25] S. Luo, X. Tan, S. Fang, et al., Adv. Funct. Mater. 26 (2016) 2826–2835.
[26] Z. Xu, M.X. Zhang, Y. Xu, et al., Sensor. Actuat. B: Chem. 290 (2019) 676–683.
[27] Y. Zou, M. Li, T. Xiong, et al., Small 16 (2020) e1907677.
[28] J. Karges, U. Basu, O. Blacque, H. Chao, G. Gasser, Angew. Chem. Int. Ed. 58 (2019) 14334–14340.
[29] S. Liu, G. Feng, B.Z. Tang, B. Liu, Chem. Sci. 12 (2021) 6488–6506.
[30] J. Zhao, K. Xu, W. Yang, Z. Wang, F. Zhong, Chem. Soc. Rev. 44 (2015) 8904–8939.
[31] K. Kiyose, S. Aizawa, E. Sasaki, et al., Chemistry 15 (2009) 9191–9200.
[32] V.N. Nguyen, S. Qi, S. Kim, et al., J. Am. Chem. Soc. 141 (2019) 16243–16248.
[33] K. Wen, H. Tan, Q. Peng, et al., Adv. Mater. 34 (2022) e2108146.
[34] X. Zhang, X. Li, W. Shi, H. Ma, Chem. Commun. 57 (2021) 8174–8177.
[35] X. Zhao, S. Long, M. Li, et al., J. Am. Chem. Soc. 142 (2020) 1510–1517.